Surface Science Approach to Photochemistry of TiO_2

Akira Sasahara[1,a] and Hiroshi Onishi[2,b]

[1]School of Materials Science, Japan Advanced Institute of Science and Technology
Nomi, 923-1292, Japan
[2]Department of Chemistry, Faculty of Science, Kobe University
Nada-ku, Kobe 657-8501, Japan
[a]sasahara@jaist.ac.jp, [b]oni@kobe-u.ac.jp

Keywords: titanium dioxide, photochemistry, temperature programmed desorption, scanning tunneling microscope, Kelvin probe force microscope

Abstract

Surface science studies of photochemistry on titanium dioxide (TiO_2) were reviewed. In the studies, photochemical processes were investigated in relation to atomic-scale surface structures by applying surface-sensitive analytical methods to single crystal TiO_2 surfaces with well-defined structures. It is demonstrated that a surface science approach is promising for full description of the photochemical processes on TiO_2.

Why a Surface Science Approach?

The present paper focuses on photochemistry studies of titanium dioxide (TiO_2) single crystal surfaces, in which photoreaction kinetics and dynamics were investigated using surfaces with atomically well-defined structures. TiO_2 has been widely studied in the field of surface science in order to reveal origins of its properties which are suitable to industrial applications including photochemical devices such as photocatalysts and photoelectrodes. The surface science studies of TiO_2 have been featured in the pioneering book of metal oxide surfaces written by Henrich and Cox published in 1994 [1] and reviewed in the paper written by Diebold in 2003 [2]. Photochemistry studies of TiO_2 were reviewed by Linsebigler et al. in 1996 with detailed instructions on surface photochemistry [3].

Titanium dioxide is a wide band gap metal oxide with a band gap of approximately 3 eV and becomes an n-type semiconductor when donor-like O vacancies are formed by reduction treatment. Irradiation by ultraviolet (UV) light causes band gap excitation to form conduction band electrons and valence band holes. A major factor showing that TiO_2 has an excellent performance as a photochemical device is the conduction and valence band edge energies appropriate for exchange of electrons with adsorbates [4]. The band bending in the vicinity of the semiconducting TiO_2 surface contributes to the photochemistry of TiO_2 by promoting the separation of the photogenerated electrons and holes. In addition to such collective properties, atomic-scale surface structures are thought to be closely related to photochemical properties of the TiO_2 [5]. Distribution of photogenerated electrons and holes should be sensitive to the local electrostatic potential influenced by arrangement of ionic Ti and O atoms. Electron transfer between adsorbates and TiO_2 surface through the overlapping orbitals should be affected by the geometric and electronic structures of the adsorbate-TiO_2 interface. Examining photochemical properties of TiO_2 surfaces in relation to their atomic-scale structures would provide unequivocal understanding of the photochemical processes. Surface science studies, where single crystal surfaces with well-defined structures are examined in controlled environments, could provide such information about the atomic-scale surface structures.

Rutile TiO_2(110) Surface; A Prototype for Surface Science Studies of TiO_2

Titanium dioxide has three natural crystal phases, anatase, brookite, and rutile. Surface science studies of TiO_2 have concentrated on the rutile crystal [2], because a large size and high quality rutile crystal is commercially available. Among the low index surfaces of the rutile TiO_2, the

(110) surface has been most widely used in surface science studies. The (110) surface exhibits a simple truncation of the bulk structure by conventional cleaning procedures in ultra-high vacuum (UHV), i.e., repetition of Ar^+ sputtering and annealing at 900 K [6]. The cleaning operation gives rise to the O vacancies and thereby raises bulk conductivity, which is beneficial for surface-sensitive analytical methods using charged particles such as electrons and ions as probes. The studies introduced here were all performed in UHV using the rutile (110) surface except for one. A brief look at the non-reconstructed (1×1) structure of the (110) surface would help us to review the studies.

Figure 1(a) shows the unit cell of the rutile crystal. The lattice constants of the tetragonal unit cell, *a* and *c*, are 0.46 and 0.30 nm, respectively. Each Ti atom is coordinated to six O atoms, and each O atom is coordinated to three Ti atoms. Figure 1(b) shows the structure of the TiO_2(110)-(1×1) surface with a unit cell of 0.65 nm×0.30 nm. The topmost O atoms are bound to two 6-fold-coordinated Ti atoms in a bridging coordination (bridging O atoms) and form rows along the [001] direction. Between the bridging O atom rows, Ti atoms coordinated to five O atoms (5-fold-coordinated Ti atoms) are exposed. A few percent of the bridging O atoms are missing [7], whereas removal of the in-plane O atoms is less probable [8]. The removed bridging O atom leaves two electrons, and the bridging O vacancies are recognized as a Ti^{3+} shoulder at the low binding energy side of the Ti $2p_{3/2}$ X-ray photoelectron spectroscopy (XPS) peak [9, 10]. In an electron energy loss (EEL) spectrum, an energy loss peak attributed to electron excitation from the O vacancy state to the conduction band appears at around 0.8 eV [10, 11]. Hydrogen atoms, possibly formed by dissociation of residual water molecules in a vacuum chamber, reside on some of the bridging O atoms and form surface hydroxyl (OH) groups [12]. The surface free from the bridging O vacancy can be prepared by 1000 K annealing in O_2 and subsequent cooling to room temperature in O_2 of the sputter-annealed (1×1) surface [9].

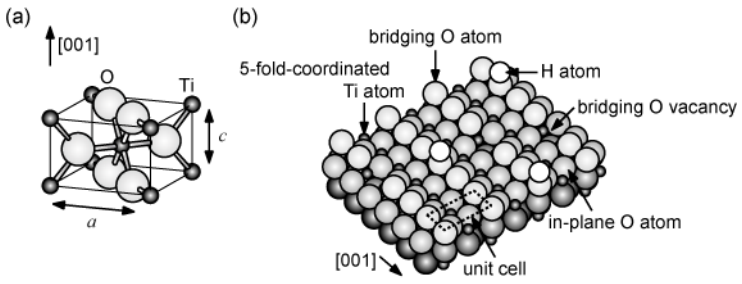

Figure 1 (a) A unit cell of the rutile TiO_2. Small and large balls represent Ti and O atoms, respectively. The lattice constants of the tetragonal unit cell, *a* and *c*, are 0.46 and 0.30 nm, respectively. (b) A ball

model of the rutile TiO_2(110)-(1×1) surface prepared by sputter-anneal cycles in UHV. Oxygen atoms are shaded according to their depth. The size of the unit cell is 0.65 nm×0.30 nm.

Atomic-Scale Observation of a TiO_2(110)-(1×1) Surface

The atomic-scale structure of the (1×1) surface can be visualized by using a scanning probe microscope (SPM). Figure 2 shows a typical (a) scanning tunneling microscope (STM) image [13] and (b) a noncontact atomic force microscope (NC-AFM) image of the (1×1) surface obtained in UHV [7]. The empty state STM image shows atomically flat terraces separated by single steps. The bright rows extending to the [001] direction correspond to the positions of the 5-fold-coordinated Ti atoms [14, 15]. The electron tunneling to the empty states derived mainly from the Ti 3d orbitals is responsible for the image contrast. The spot indicated by the circle A between the neighboring Ti atom rows is the bridging O vacancy. The surface OH groups are occasionally observed as spots between the Ti atom rows [12, 16], possibly depending on the tip condition, though they are not observed in Fig. 2(a). The depression in the Ti atom rows B was assigned to subsurface defects in ref. 13. The NC-AFM, a scanning probe microscope which regulates the tip-sample distance by detecting weak attractive force [17], visualizes the geometrically higher bridging O atom rows as bright rows as shown in Fig. 2(b). The depressions in the rows are the bridging O vacancies. The surface OH groups are occasionally observed as protrusions or depressions on the rows dependent on the polarity of the tip end [18, 19].

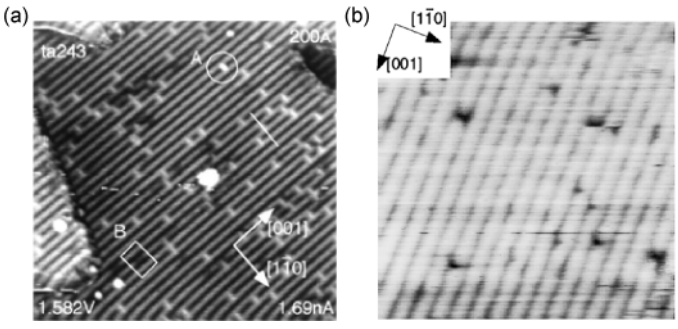

Figure 2 (a) An empty state STM image of the rutile TiO_2(110)-(1×1) surface (20 nm×20 nm) [13]. Sample bias voltage (V_s) = +1.582 V, tunneling current = 1.69 nA. (b) An NC-AFM image of the TiO_2(110)-(1×1) surface (10 nm×10 nm) [7]. Frequency shift (Δf) = -80 Hz, V_s = 0 V.

Photochemistry of Oxygen

Surface species derived from the O_2 molecule such as superoxide anion radical (O_2^-) and atomic oxygen play key roles in the photoreactions on powdered TiO_2 [20, 21]. The possible roles of the

oxygen species include an oxidizer, a trap for photogenerated electrons, and maintaining of the stoichiometry of the TiO_2 surface. Clarifying the behaviors of the oxygen species is prerequisite for understanding photochemical processes on TiO_2 surfaces.

The first report examining photochemistry of oxygen species on the rutile TiO_2(110)-(1×1) surface was by Lu et al. [22, 23]. The surface was exposed to O_2 at 105 K, and photodesorbed species were examined. Irradiation by UV light with energy larger than the band gap of the TiO_2 (3.1 eV) induced desorption of O_2 molecules, whereas thermal desorption of O_2 did not occur at the temperature between 100 and 500K. The maximum yield of O_2 was comparable to the number of the bridging O vacancies titrated by low energy ion scattering techniques. An equivalent amount of $^{16}O_2$ and $^{18}O_2$ was desorbed from the surface exposed to an equivalent mixture of $^{16}O_2$ and $^{18}O_2$. The authors concluded that the O_2 molecules were adsorbed at the bridging O vacancies and were desorbed by capturing photogenerated holes. The molecularly adsorbed oxygen species were designated as α-O_2. From detailed analysis of the photodesorption spectra, the α-O_2 was distinguished between two species with different desorption cross sections, α_1-O_2 and α_2-O_2 [24]. The α_1-O_2 and α_2-O_2 were assigned to the molecular oxygen species in different types of O vacancies. Heating the surface to 200 K with the α-O_2 gave rise to a new component with a faster desorption rate in the O_2 photodesorption spectra. This was attributed to the conversion of the α-O_2 to another molecular species, β-O_2. Superoxide anion radical and peroxide anion (O_2^{2-}) formed by electron transfer from the reduced Ti atoms to the O_2 molecules were proposed as candidates for the α-O_2 and the β-O_2. Photodesorption of the β-O_2 decreased as the heating temperature was raised and completely ceased by heating to temperatures above 400 K, which indicated dissociation of the β-O_2 to O atoms. One O atom filled the vacancy, and the other resided on the Ti atom rows [16, 25, 26]. The transition of the oxygen species on the TiO_2(110)-(1×1) surface is illustrated in Fig. 3(a).

Perkins et al. reported the photochemical property of the O adatoms on the TiO_2(110)-(1×1) surface [27]. Figure 3(b) shows the temperature programmed desorption (TPD) spectra of H_2O from the surface. Spectrum a obtained on the surface exposed to H_2O at 115 K showed two peaks at 270 and 520 K. The peak at 270 K arose from H_2O molecularly adsorbed on the 5-fold-coordinated Ti atoms [25], and the peak at 520 K was assigned to the H_2O produced by recombination of two OH groups which were formed by dissociative adsorption of H_2O molecules at the bridging O vacancies [28]. Spectrum b was obtained on the surface exposed to O_2 and then to H_2O at 115 K. The shoulder on the high temperature side of the peak at 270 K originated from

H_2O produced by recombination of two OH groups on the 5-fold-coordinated Ti atoms, and indicates the presence of the O adatoms. A H_2O molecule reacts with the O adatom to form two OH groups [25]. The peak at 520 K in spectrum a disappeared because the bridging O vacancies were filled by the O_2 dose. Spectrum c was obtained on the surface which was exposed to O_2 at 115 K, irradiated by UV light ($h\nu$ = 4.13 eV), and then exposed to H_2O. The existence of the shoulder indicated that the O adatoms remained on the surface after UV irradiation.

In summary, molecular oxygen and atomic oxygen are possible oxygen species on the TiO_2(110)-(1×1) surface. The molecular species α-O_2 is formed in the bridging O vacancy at 105 K, and is converted to other oxygen species, β-O_2 and O adatoms, at higher temperatures. The α-O_2 and β-O_2 are desorbed with the band gap excitation of TiO_2 at temperatures higher than 105 K. The O adatoms remain on the surface after UV irradiation at 115 K.

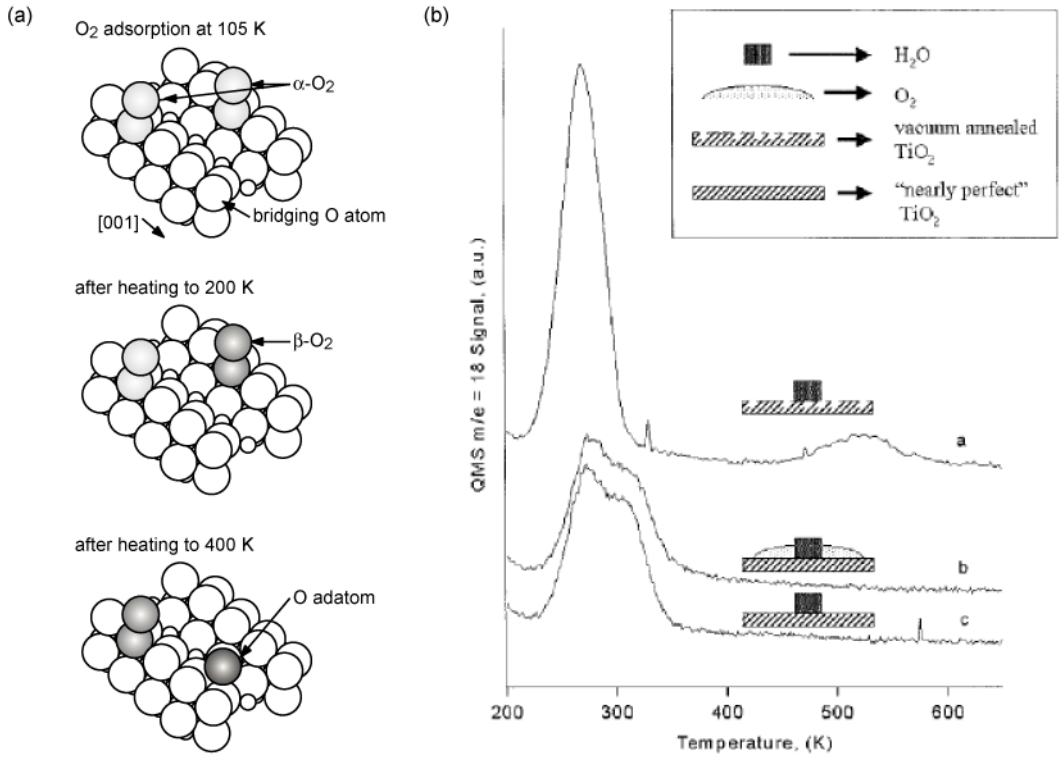

Figure 3 (a) A schematic illustration representing the oxygen species on the TiO_2(110)-(1×1) surface. (b) The TPD spectra of H_2O from the TiO_2(110)-(1×1) surfaces. a: The surface exposed to H_2O at 115 K. b: The surface exposed to O_2 and then to H_2O at 115 K. c: The surface exposed to O_2, irradiated by UV ($h\nu$ = 4.13 eV), and then exposed to H_2O [27].

Photooxidation of Carbon Monoxide

Oxidation of carbon monoxide (CO) is a prototypical model reaction widely studied in the field

of surface science [29] due to its relative simplicity and importance from the view point of industrial applications such as air pollution control catalysts, gas sensors, and fuel cells.

Linsebigler et al. examined photooxidation of $C^{18}O$ on the rutile TiO_2(110)-(1×1) surface [23, 24, 30]. The surface was exposed to $^{18}O_2$ and then $C^{18}O$ at 105 K, and desorption of $C^{18}O_2$ induced by UV irradiation ($h\nu$ = 3.9 eV) was monitored. $C^{18}O_2$ was desorbed when the vacancy-free (1×1) surfaces were annealed at temperatures higher than 400 K prior to the exposure to $^{18}O_2$, and the yield of $C^{18}O_2$ increased with the temperature of the pre-annealing. The $C^{18}O_2$ desorption was not observed when the vacancy-free surfaces were not annealed or were Ar^+ sputtered. The results indicated that the bridging O vacancy was needed for the CO_2 production. The exponential decay constant for the CO_2 desorption was identical to that of the α-O_2 photodesorption, and the yield of CO_2 decreased with the conversion of the α-O_2 to the β-O_2. Exclusive production of $C^{18}O_2$ from $C^{18}O$ and $^{18}O_2$ excluded the involvement of the lattice O of the TiO_2 in the reaction, and exclusive production of $C^{18}O^{16}O$ from $C^{18}O$ and $^{16}O_2$ excluded the dissociation of CO in the reaction. The authors concluded that the CO_2 was produced by photochemical reaction of the α-O_2 with the CO molecularly adsorbed on the 5-fold-coordinated Ti atom [31]. The CO photooxidation was a minor process compared to that of the O_2 photodesorption.

Linsebigler et al. reported the effect of Pt loading on the CO photooxidation as well [32]. It is known that loading nanometer-sized Pt clusters is effective for enhancing the photocatalytic activity of powdered TiO_2 [33]. After Pt evaporation using a Pt wire as a source, the TiO_2(110)-(1×1) surface was annealed at 600 K to promote clustering of Pt and to generate the bridging O vacancies. The surface was exposed to $^{18}O_2$ and then to $C^{18}O$ at 105 K, and photodesorption of $C^{18}O_2$ was monitored. The left-hand panels in Fig. 4 show the photodesorption spectra of $C^{18}O_2$ from the surface containing different amounts of Pt under UV irradiation ($h\nu$ = 3.9 eV). The initial rate of $C^{18}O_2$ production (height of the initial peak of the desorption spectrum) and yield of the $C^{18}O_2$ (peak area) were both reduced with the amount of Pt, which was attributed to a decrease of the bare TiO_2 surface providing bridging O vacancies. The exponential decay constants for the $C^{18}O_2$ desorption were independent of the Pt loading as shown in the right-hand panel. Thus the Pt loading was ineffective on CO photooxidation on the TiO_2(110) surface at a low temperature where thermal processes are quenched.

It was shown that α-O_2 was the active species for CO photooxidation on the TiO_2(110)-(1×1) surface at 105 K and that the kinetics of the photooxidation was insensitive to the Pt loading at that temperature. The activity of O adatoms on CO photooxidation and the role of Pt clusters at higher

temperatures would be an interesting subject for further investigation.

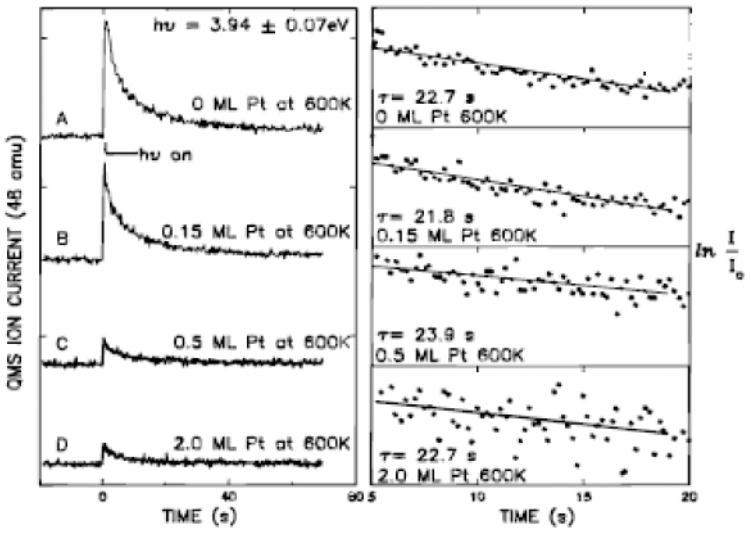

Figure 4 Kinetics of CO_2 production for $CO+O_2$ layers on Pt-loaded TiO_2(110)-(1×1) surfaces. Left panel: photodesorption spectra of CO_2. Right panel: decay times for CO_2 formation rate derived from the spectra in the left panel. One monolayer (ML) of the Pt was defined to be 1.5×10^{15} cm^{-2} [32].

Photochemistry of Halomethanes

Halomethanes ($CH_{4-n}X_n$, X=F, Cl, Br) are frequently used in photochemical studies [34, 35]. The molecules have a strong absorption in the UV region, and their simple structures are beneficial for identifying reaction intermediates and products.

Weitz and co-workers studied the photochemistry of deuterated iodomethane (CD_3I) on the rutile TiO_2(110)-(1×1) surface [36, 37]. A vacancy-free (1×1) surface with 1 ML (1 ML = 3.8×10^{14} cm^{-2}) of CD_3I was prepared by exposing the surface to CD_3I gas at 100 K and was irradiated by UV light with the wavelengths of 257-351 nm. Analysis of photodesorbed species by time-of-flight mass spectroscopy showed that dissociation was predominant over the molecular desorption of the CD_3I. Complete loss of the C 1s XPS peak by UV irradiation indicated that the CD_3 fragments were expelled to the gas phase and did not remain on the surface. The dissociation cross section was estimated from the intensities of C 1s and I $3d_{5/2}$ XPS peaks originating from the CH_3I molecules on the surface. The I $3d_{5/2}$ peak originating from the CD_3I molecule exhibits higher binding energy than that from I adatoms by 1.6 eV. The estimated cross section was equivalent to the photodissociation cross section of gas phase CD_3I when the wavelength of UV light was shorter than 302 nm. The authors concluded that the contribution of the photogenerated electrons and

holes to the CD_3I dissociation was limited due to poor overlap of electronic states between the adsorbed CD_3I molecules and the TiO_2 surface, and that the CD_3I molecules were directly excited by the UV irradiation. When the wavelengths of UV light were longer than 334 nm, the photodissociation cross sections on the TiO_2 surface exceeded that in the gas phase. This was explained by the contribution of TiO_2 becoming relatively large due to reduced UV absorption by the CD_3I molecule.

Yates, Jr. and co-workers reported photooxidation of chloromethane (CH_3Cl) on the TiO_2(110)-(1×1) surface [38, 39]. The surface was exposed to reactant gases at 105 K, and the species remaining on the surfaces after UV irradiation was identified by TPD. Figure 5 shows the yield ratios of the species. No species except for CH_3Cl was desorbed from the vacancy-free surfaces and the surfaces exposed only to $D_2{}^{18}O$ (upper scheme). When the surface was exposed to $^{18}O_2$ prior to the CH_3Cl exposure, $H_2{}^{18}O$, $C^{18}O$, and formaldehyde (70% $H_2C^{18}O$ and 30% $H_2C^{16}O$) were detected with a decrease of CH_3Cl (middle scheme). When the surface was exposed consecutively to $D_2{}^{18}O$, $^{16}O_2$, and CH_3Cl, the desorption yield ratio of the $H_2C^{18}O$ and $H_2C^{16}O$ was reversed, and $C^{16}O$ was not detected (lower scheme). Hydrogen chloride (HCl) was another product which showed a delayed increase after the photooxidation experiments due to its low yield and high sticking probability on the chamber walls. Neither desorption nor fragmentation of the CH_3Cl occurred during the UV irradiation in each experiment. The authors concluded that the bridging O vacancies and O_2 exposure were essential to the photooxidation of CH_3Cl and that the surface OH groups derived from H_2O were not. Direct reaction of the oxygen species with the CH_3Cl to produce CO was proposed on the basis of the fact that the O atoms of CO were derived exclusively from O_2. The oxygen species is possibly the α-O_2. The O_2, H_2O, and TiO_2 were all possible sources of the O atom in H_2CO, which indicated that the reaction path to produce H_2CO was different from that for the CO production.

Contribution of the vacancy-free TiO_2 surface to the CD_3I photodissociation seems important. The step edges are possible surface structures which enhance dissociation. Coordination to the 4-fold-coordinated Ti atoms exposed at the step edges [13] might allow better electronic overlap for the CD_3I molecules compared to the 5-fold-coordinated Ti atoms on the flat terraces. Employing high index surfaces with high density of steps [40] would clarify the contribution of the steps to the photooxidation.

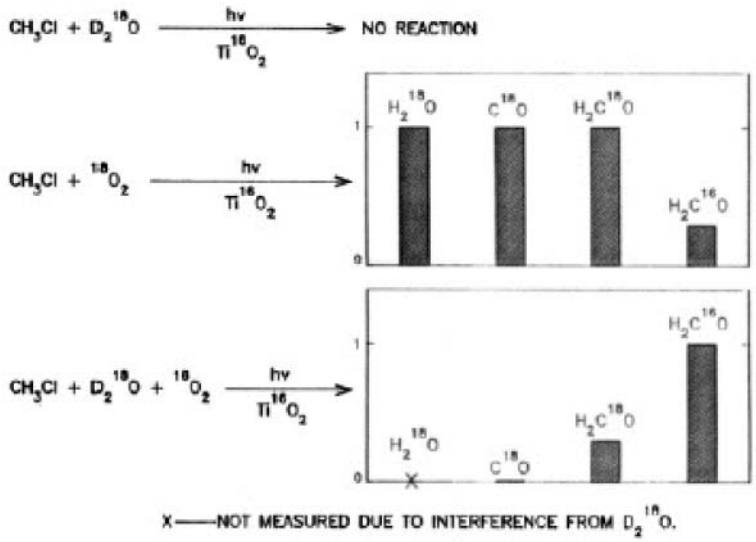

Figure 5 The isotope distribution in the photochemical products on TiO_2(110)-(1×1) surface [38].

Photooxidation of Acetone

Acetone (CH_3COCH_3), often used as ingredients in household products such as glues, paints, and varnishes, potentially causes headaches, fatigue, and nausea, and is one of the volatile organic chemicals which should be reduced by TiO_2 photocatalysts.

Henderson examined photooxidation of acetone on the TiO_2(110)-(1×1) surface [41]. The surface was exposed to acetone at 95 K, and TPD analysis was performed on surfaces with 0.25 and 1 ML (1 ML = 5.2×10^{14} cm^{-2}) of acetone to examine the species remaining on the surface. After irradiation with a Hg arc lamp in O_2 at 95 K, the peak of the TPD of a ketene (CH_2=C=O) grew with the decrease of the peak of acetone as the irradiation time was extended. Desorption of the ketene indicated the presence of acetate (CH_3COO^-) which is thermally decomposed to ketene during the TPD. In the photodesorption spectra on surfaces with 0.75 ML of acetone at 200 K, desorption of methyl radicals (CH_3) was confirmed. The cross section of the CH_3 desorption was equivalent to the depletion cross section of the adsorbed acetone estimated from its coverage determined from the TPD peak intensities. The conversion of acetone to the acetate with a cleavage of the C-C bond was concluded. The left panel of Fig. 6 shows CH_3 photodesorption spectra obtained on the surfaces covered by 0.25 ML of acetone at 105 K. The CH_3 was not detected on the surface exposed only to acetone as shown in spectrum (a). When the surface was exposed to O_2 at 95 K and heated to room temperature prior to the exposure to acetone, CH_3 desorption was observed as shown in (b). Heating the surface used in (b) up to 243 K before UV irradiation gave rise to an over 4-fold increase of the initial yield of the CH_3 (a component with a

faster desorption rate forming the initial spike) as shown in (c). The results indicated the need of O_2 and the presence of thermal activation barrier in the acetone photooxidation process. The author proposed a process via the intermediate formed by thermal reaction of the acetone and active oxygen species (either O adatom or O_2 molecules). A linear chain of acetone molecules anchored to the 5-fold-coordinated Ti atom rows and ended by an O adatom was presented as a candidate for the complex [42]. The photooxidation process is illustrated in the right panel of Fig. 6.

Lateral distribution of the complex and its conversion to acetate might be visualized by scanning probe microscopes. The STM [43] and NC-AFM [44] offer sufficiently high spatial resolution to identify individual carboxylate molecules ($R\text{-}COO^-$, R = H, CH_3, $(CH_3)_3C$, $HC{\equiv}C$, CF_3, CF_2H) on the TiO_2 surface as spots with different image heights.

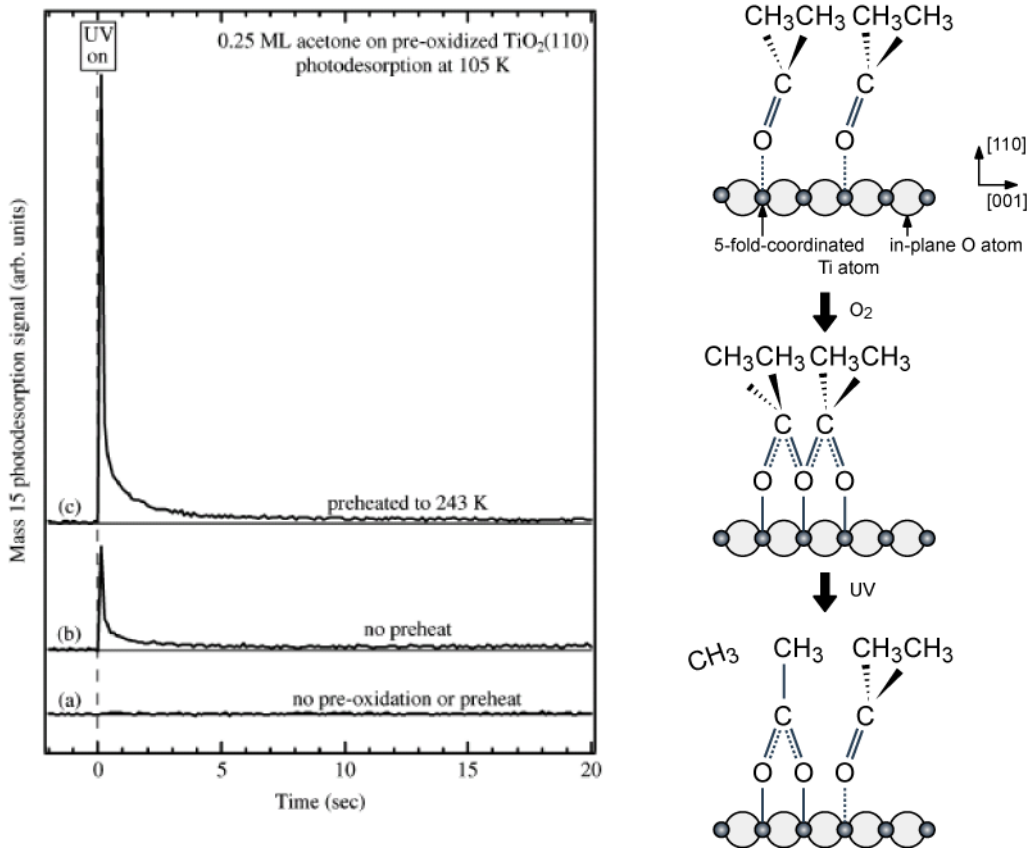

Figure 6 Left panel: photodesorption spectra of methyl radical on the TiO_2(110) surfaces at 105 K. (a) Surface exposed only to acetone at 105 K. (b) Surface exposed to O_2 at 95 K, heated to room temperature, and cooled to 105 K for acetone adsorption. (c) Surface (b) heated to 243 K and cooled to 105 K after the acetone adsorption [41]. Right panel: a schematic illustration representing photooxidation of acetone on the TiO_2(110) surface.

Photodehydrogenation of 2-Propanol

2-propanol is one of the probe molecules used to assess catalytic activity and examine reaction dynamics [45, 46]. A rich store of knowledge from previous catalysis research is beneficial when examining the reaction dynamics on model surfaces.

Brinkley et al. examined photoreaction of 2-propanol ($CH_3CHOHCH_3$) on the TiO_2(110)-(1×1) surface [47, 48]. Mixed gas of 2-propanol and O_2 was introduced to the TiO_2 surface, and the products in the reflected gas were examined. When the surface was irradiated by UV light ($h\nu$ = 3.1-4.1 eV), acetone and H_2O were produced with a ratio of 1:1. The reaction probability per collision of the 2-propanol was 0.15. The authors proposed a process in which the trap of the photogenerated electrons by adsorbed O_2 molecules (reaction (1)) initiated the dehydrogenation of the 2-propanol. The holes were efficiently trapped by the 2-propanol, which reduced the barrier to remove H atoms of the OH group to produce the reaction intermediate $CH_3(CHO)CH_3$ (reaction (2), (3)). The intermediate was dehydrogenated by OH groups including the bridging O atoms or those on 5-fold-coordinated Ti atoms (reaction (4), (5)).

$$O_2\,(a) + e^- \rightarrow O_2^-\,(a) \quad (1)$$

$$CH_3CHOHCH_3\,(a) + h^+ \rightarrow CH_3(CHOH)^+CH_3\,(a) \quad (2)$$

$$CH_3(CHOH)^+CH_3\,(a) + Ti^{4+}\text{-}O^{2-}\text{-}Ti^{4+} \rightarrow CH_3(CHO)CH_3\,(a) + Ti^{4+}\text{-}OH^-\text{-}Ti^{4+} \quad (3)$$

$$CH_3(CHO)CH_3\,(a) + Ti^{4+}\text{-}OH^-\text{-}Ti^{4+} \rightarrow CH_3COCH_3\,(a) + H_2O\,(a) + Ti^{3+}\text{-}[\ ]\text{-}Ti^{4+} \quad (4)$$

$$CH_3(CHO)CH_3\,(a) + Ti^{4+}\text{-}OH^- \rightarrow CH_3COCH_3\,(a) + H_2O\,(a) + Ti^{3+} \quad (5)$$

The designation "(a)" and the bracket stand for an adsorbed species and the bridging O vacancy, respectively. The reaction probability of the 2-propanol increased when the (1×1) surface was annealed prior to the reaction. The increase of the reaction probability was attributed to an enhanced adsorption of O_2 and 2-propanol in the bridging O vacancies. Figure 7 shows the reaction probability on the surface pre-annealed at 800 K as a function of exposure time to the mixed gas. The reaction probability decreased from 0.15 to 0.09 when O_2 exposure reached 5×10^3 ML (1 ML = 5.2×10^{14} cm^{-2}). The authors concluded that the decrease of the reaction probability was due to healing of the bridging O vacancies and that the vacancy-free surface was active for the dehydrogenation of the 2-propanol. The surface defects insensitive to the oxidation such as steps and subsurface O vacancies were proposed as possible active sites.

Contribution of subsurface O vacancies to the photochemical reactions, as well as the activity of step edges which was mentioned also in the sections about halomethanes, is an issue to be examined.

Titanium dioxide wafers with a controlled dopant concentration might provide some insights into the influence of subsurface defects [49].

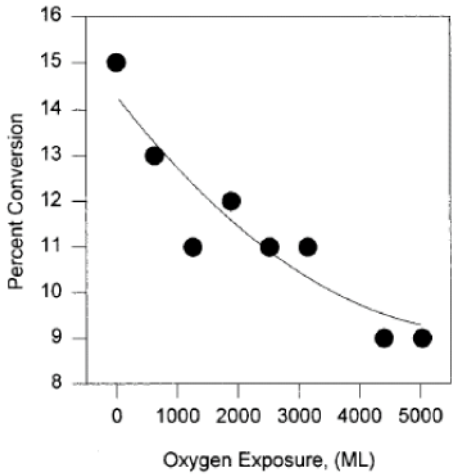

Figure 7 Reaction probability of 2-propanol to acetone in a steady state as a function of exposure time to 2-propanol and O_2 flux under UV irradiation at 350 K. 2-propanol = 0.1 ML s^{-1}, O_2 = 0.7 ML s^{-1} [48].

Photodecomposition of Pivalate

Lateral charge distribution on TiO_2 surface is an important issue closely related to photochemical processes which involve transfer and trapping of photogenerated electrons. Scanning probe microscopes, which detect tip-sample interaction such as tunneling current and atomic force, are powerful analytical tools for atomic-scale surface analysis.

Henderson et al. examined photodecomposition of pivalate ($(CH_3)_3CCOO^-$) adsorbed on the TiO_2(110)-(1×1) surface at 280 K [50-52]. A sequence of the STM image at each experimental stage is presented in the left panel of Fig. 8. Image (a) shows the (1×1) surface with the bridging O vacancies of 0.12 ML (1 ML = 5.2×10^{14} cm^{-2}). The bright lines diagonally crossing the image from the top left to the bottom right are the Ti atom rows, and the spots between the rows are the bridging O vacancies. After exposure to O_2, 0.09 ML of the vacancies disappeared in the image, and an equivalent number of spots appeared on the Ti atoms rows as shown in image (b). The spots were assigned to O adatoms. Image (c) shows the surface (b) exposed to pivalic acid ($(CH_3)_3CCOOH$) gas at room temperature. Individual spots arranged in a (2×1) periodicity (0.60 nm × 0.65 nm) are the pivalates. The pivalic acid molecule dissociates to the pivalate anion and H^+ on the TiO_2(110)-(1×1) surface. The pivalates are anchored to two 5-fold-coordinated Ti atoms in a bridge form and are saturated at 0.5 ML. The accompanying H^+ forms a surface OH group on the bridging O atom [53].

$$(CH_3)_3CCOOH + Ti^{4+}\text{-}O^{2-}\text{-}Ti^{4+} \rightarrow (CH_3)_3CCOO^- + Ti^{4+}\text{-}OH^-\text{-}Ti^{4+} \quad (6)$$

A model of the pivalate-adsorbed surface is represented in the right panel of Fig. 8. After irradiation by a Xe arc lamp for 1 hour, 0.33 ML of the pivalates disappeared, and faint spots of 0.17 ML appeared between the Ti atom rows as shown in images (d) and (e). The faint spots were assigned to OH groups bound to 6-fold-coordinated Ti^{3+} cations which resulted from trapping of the photogenerated electrons. The increase of the Ti^{3+} was monitored by the growth of a broad feature with a maximum at around 0.8 eV in EEL spectra. During the irradiation, an equivalent amount of CO_2 and isobutene ($(CH_3)_2C=CH_2$) was yielded. After re-exposure to O_2, the faint spots in STM images disappeared as shown in image (f), and the broad range in the EEL spectra was reduced. The reaction process was proposed as follows:

$$(CH_3)_3CCOO^- + h^+ \rightarrow (CH_3)_3C + CO_2 \quad (7)$$

$$Ti^{4+}\text{-}OH^-\text{-}Ti^{4+} + e^- \rightarrow Ti^{3+}\text{-}OH^-\text{-}Ti^{4+} \quad (8)$$

$$Ti^{3+}\text{-}OH^-\text{-}Ti^{4+} + 1/4O_2 \rightarrow Ti^{4+}\text{-}O^{2-}\text{-}Ti^{4+} + 1/2H_2O \quad (9)$$

Uetsuka et al. examined the effect of the Pt loading on the photodecomposition of the pivalate on the TiO_2(110)-(1×1) surface [54]. Nanometer-sized Pt clusters were prepared on the surface by Pt evaporation followed by annealing at 920 K. On Pt-free surfaces, the initial rate of the pivalate decomposition, which was estimated from the coverage of adsorbed pivalates in the STM images, was 0.4 ML h^{-1} (1 ML = 2.6×10^{14} cm^{-2}) at 280 K. The decomposition stopped when 0.4 ML of the pivalates was consumed. The decomposition rate and the maximum consumption of the pivalate increased with the amount of Pt, and reached 1.2 ML h^{-1} and 0.8 ML, respectively, with the Pt clusters of 8×10^{11} cm^{-2}. The enhanced decomposition was attributed to the electron trapping of the Pt clusters. Hiehata et al. reported an increase of the work function on the Pt clusters on the TiO_2(110)-(1×1) surface after the photodecomposition of the pivalate by using a Kelvin probe force microscope (KPFM) [55]. The KPFM is an applied method of the NC-AFM and provides a lateral distribution of the work function with the surface topography [17, 56, 57]. The work function increase was attributed to the enhanced dipole moment component directed from the vacuum to the surface by electron accumulation to the Pt clusters.

The studies demonstrated that the photogenerated electrons and holes can be tracked in relation to atomic-scale surface structures on the well-defined TiO_2 surfaces. Controlling the charge distribution on the basis of surface structures such as surface defects, metal cluster sizes, and

intercluster distances might be one possible way to optimize the performance of photochemical devices.

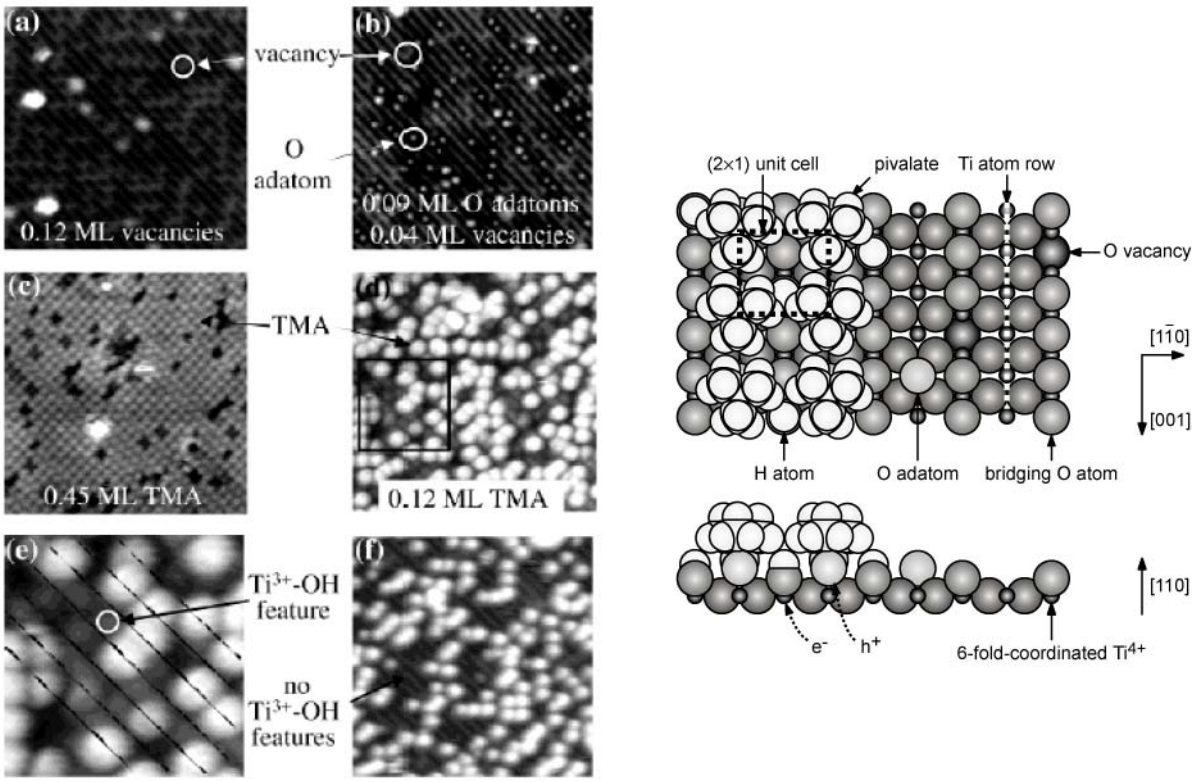

Figure 8 Left panel: STM images of TiO_2(110) surfaces at 280 K. (a) The TiO_2(110)-(1×1) surface. (b) The surface in (a) exposed to 100 L of O_2. (c) The surface in (b) after exposure to pivalic acid gas. (d) The surface in (c) after UV irradiation in UHV for 1 h. (e) Close up of the region indicated by a square in (d). (f) The surface shown in (d) after exposure to 100 L of O_2. Size of the images is 16 nm×16 nm with exception of image (e) [50]. Right panel: Schematic illustration representing the pivalate-covered surface.

Electron Transfer from Dye Molecule to TiO_2

Anodes of dye-sensitized solar cells are one of the major applications of TiO_2 [58, 59]. Electron transfer through overlapping molecular orbitals of the dye and TiO_2 surface is a key step in the solar-to-electricity conversion process and should be controlled by how and where the dye is adsorbed on the surface. However, there has been no way of examining the electron transfer for individual dyes.

Ikeda et al. performed work function measurement on Ru(4,4'-dicarboxy-2,2'-bipyridine)$_2$(NCS)$_2$ (N3) dye-adsorbed TiO_2(110) surfaces by using the KPFM [60]. The TiO_2(110)-(1×1) surface was removed from the vacuum chamber after exposure to pivalic acid gas and was immersed in the

solution of the N3. The pivalate monolayer protects the (1×1) surface against contaminants from the laboratory air [61]. The set of images in Fig. 9(a) shows the topography and simultaneously obtained work function map of the N3-adsorbed surface in the dark. Bright particles in the topographic images were assigned to the N3 molecules and the aggregates which replaced the pivalates. In the work function map, the areas with larger work function were presented brighter. The work function on the N3 was larger than that on the surrounding pivalate-covered TiO_2 surface by 0.07 V on average. Under visible light irradiation, the work function on 44% of the N3 became smaller than that on the pivalate monolayer by 0.14 eV on average as shown in the images of Fig. 9(b). The authors claimed that the work function decrease was due to the enhancement of dipole moment component directed to the vacuum side, which was caused by the electron injection from the N3 to the TiO_2. A schematic illustration representing the dipole moments originating from the adsorbed molecules is shown in the right panel of Fig. 9. Trapping of the injected electrons at the 6-fold-coordinated Ti atom bound to the bridging O atoms was assumed. Otherwise, the injected electrons would have been immediately recombined with the cationized N3 molecules.

It was demonstrated that the electron transfer properties of individual dyes can be examined. Correlating the electron transfer to the atomic-scale structure of TiO_2 surfaces and adsorbed dyes may offer clues leading to enhancement of the electron injection efficiency from the dyes on the basis of the electrode surface structures and thereby improve solar cell performance.

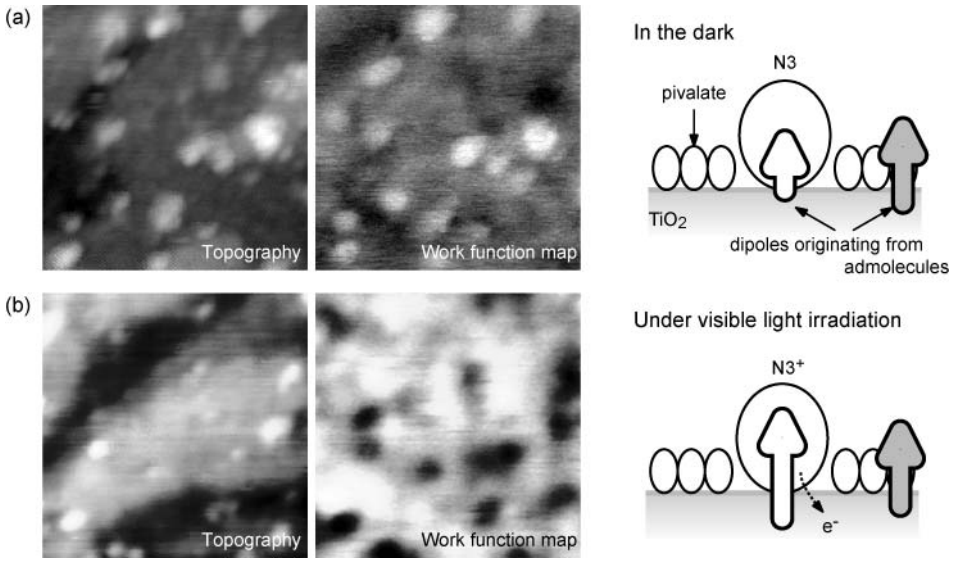

Figure 9 Left panels: Sets of topographic images and work function maps of the N3-adsorbed TiO_2(110) surfaces obtained (a) in the dark and (b) under visible light (30 nm×30 nm). Right panels: Schematic illustration representing the change of dipole moments originating from adsorbed molecules.

Photodecomposition of Acetic Acid

Band bending in the vicinity of the surface is one of the factors determining the photochemical property of semiconducting TiO_2. In the band-bending region, the photogenerated electrons and holes are separated by the electric field, and the electron-hole recombination is suppressed.

Idriss et al. examined photodecomposition of acetic acid (CH_3COOH) on a rutile TiO_2(001) surface [62, 63]. Two kinds of TiO_2(001) surfaces with different structures, the {011}-faceted surface and {114}-faceted surface [64], were prepared by flashing to 750 and 900 K in O_2, respectively, following cleaning by cycles of Ar^+ sputtering and annealing. Models of the (001), (011), and (114) surfaces assuming bulk termination are shown in Fig. 10(a). The three surfaces have different arrangements of the Ti and O atoms in the topmost layer. The surface Ti atoms are all coordinated to four O atoms on the (001) surface, but to five O atoms on the (011) surface. The (114) surface consists of both 4-fold and 5-fold coordinated Ti atoms. A steady flow of acetic acid gas was introduced to the {011}-faceted and {114}-faceted surfaces under UV irradiation ($h\nu$ = 3.4 eV) at 320 K, and products in the gas phase were examined. Ethane (C_2H_6), methane (CH_4) and CO_2 were produced on both surfaces. The formation of C_2H_6 showed a sharp initial increase due to the consumption of the lattice O atoms of TiO_2. Figure 10(b) shows the initial yield of the ethane as a function of the pressure of the acetic acid gas. The {011}-faceted surface provided a larger yield than the {114}-faceted surface did. The authors attributed the difference in activity of the two surfaces to collective properties. Assuming that the identical reaction products on the two surfaces suggested the identical reaction pathway, local arrangement of surface Ti and O atoms was thought to be insufficient to explain the difference in activity. The difference in width of the band-bending region was proposed as the origin of the different activity. The widths of the band-bending region estimated from the quantum yields of the acetic acid photodecomposition were 18.2 and 6.6 nm for the {011}-faceted and the {114}-faceted surfaces, respectively.

It was shown that the studies on well-defined surfaces highlight the contribution of the band bending to the photochemical processes on TiO_2 surface. Closer consideration of the effects of the adsorbates and the dopants as well as the arrangement of the ionic Ti and O atoms on the band bending would promote better understanding of the photochemical properties of TiO_2.

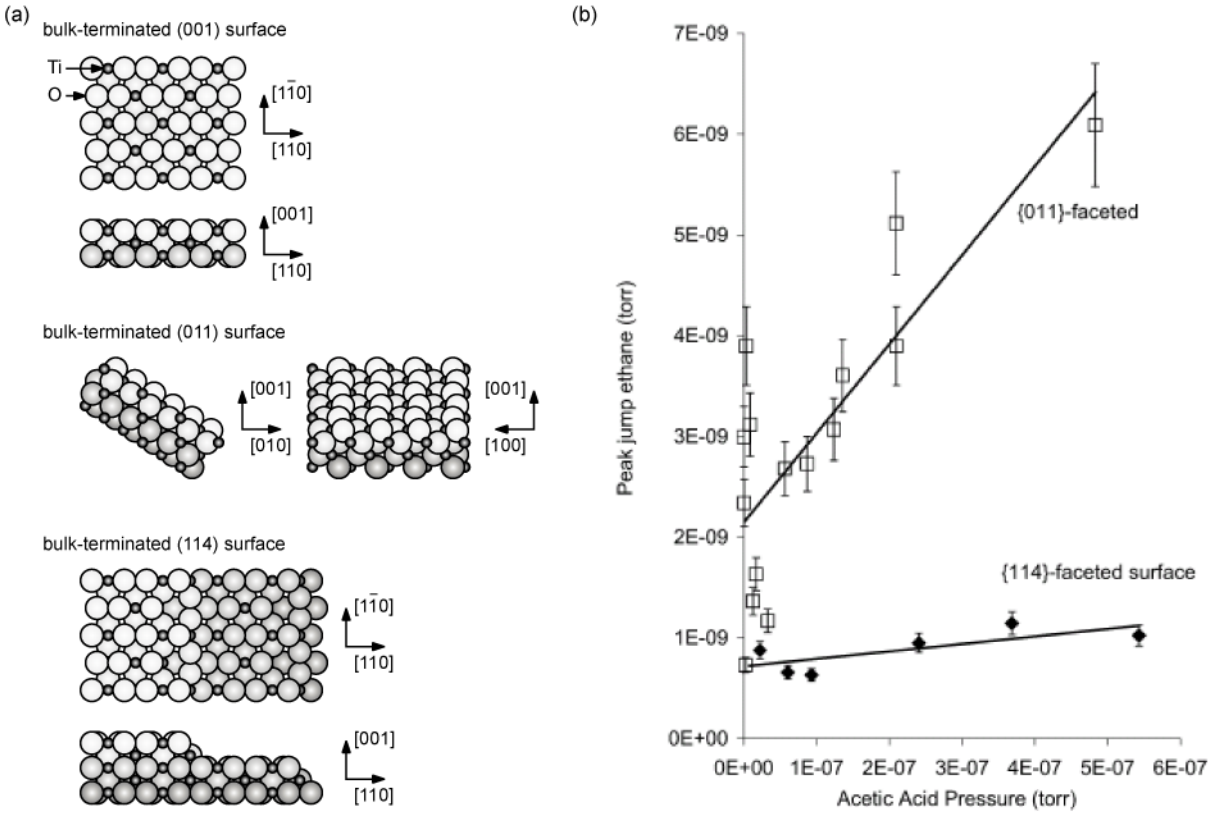

Figure 10 (a) Ball models of the rutile TiO_2(001) surface, (011) surface, and (114) surfaces. Small and large balls represent Ti and O atoms, respectively. Oxygen atoms are shaded according to their depth. (b) Formation of ethane in steady-state conditions on the {011}-faceted and {114}-faceted TiO_2(001) surfaces as a function of acetic acid pressure in an ultrahigh vacuum [63].

Outlook

The studies introduced here demonstrated that the surface science approach offers deeper insights into the photochemical processes on the TiO_2 surfaces in relation to atomic-scale surface geometry and local electronic structure. The motivations for the studies originate from the importance of the TiO_2 in industrial applications as well as pure scientific interest. A future subject is to bridge the fundamental research and industrial applications more firmly by reducing the material gap (differences between the model surfaces and the surfaces of TiO_2 in industrial uses) and the pressure gap (difference between UHV for surface science analysis and high-pressure gaseous/liquid environments for industrial application).

The use of epitaxially grown single crystalline anatase TiO_2 films [65-68] would reduce the material gap. Anatase generally shows higher performance as photocatalysts and photoelectrode in comparison to rutile. Preparation of model surfaces in accordance with surface modification methods for photochemical devices may provide novel insights. Photocatalytic activity is

sensitive to preparation conditions such as metal-loading methods and redox treatments as well as loaded metals and the loading amount [3, 69, 70]. To reduce the pressure gap, the NC-AFM is one of the promising analytical tools. Atomic scale imaging has been attained in water [71] as well as in an atmospheric pressure gas [72]. In addition to the high spatial resolution, the NC-AFM has potential to derive various tip-surface interactions. Interface-selective nonlinear optical spectroscopy [73] is another powerful analytical method for detailed description of the interface structures.

References

[1] V. E. Henrich and P. A. Cox: *The Surface Science of Metal Oxides* (Cambridge University Press, New York 1994).

[2] U. Diebold: Surf. Sci. Rep. Vol. 48 (2003), p. 53.

[3] A. L. Linsebigler, G. Lu and J. T. Yates, Jr.: Chem. Rev. Vol. 95 (1995), p. 735.

[4] A. Hagfeldtt and M. Grätzel: Chem, Rev. Vol. 95 (1995), p. 49.

[5] J. Nowotny, T. Bak, M. K. Nowotny, and L. R. Sheppard: Int. J. Hydrogen Energy Vol. 32 (2007), p. 2651.

[6] H. Onishi, K. Fukui, and Y. Iwasawa: Surf. Sci. Vol 313 (1994), p. L783.

[7] K. Fukui, H. Onishi, and Y. Iwasawa: Phys. Rev. Lett. Vol. 79 (1997), p. 4202.

[8] Q. Guo, I. Cocks, and E. M. Williams: Phys. Rev. Lett. Vol. 77 (1996), p. 3851.

[9] J. –M. Pan, B. L. Maschhoff, U. Diebold, and T. E. Madey: J. Vac. Sci. Technol. A Vol. 10 (1992), p. 2470.

[10] W. Göpel, J. A. Anderson, D. Frankel, M. Jaehnig, K. Phillips, J. A. Schäfer, and G. Rocker: Surf. Sci. Vol. 139 (1984), p. 333.

[11] M. A. Henderson: Surf. Sci. Vol. 400 (1998), p. 203.

[12] S. Suzuki, K. Fukui, H. Onishi, and Y. Iwasawa: Phys. Rev. Lett. Vol. 84 (2000), p. 2156.

[13] U. Diebold, J. Lehman, T. Mahmoud, M. Kuhn, G. Leonardelli, W. Hebenstreit, M. Schmid, and P. Varga: Surf. Sci. Vol. 411 (1998), p. 137.

[14] H. Onishi, K. Fukui, and Y. Iwasawa: Bull. Chem. Soc. Jpn. Vol. 68 (1995), p. 2447.

[15] H. Onishi and Y. Iwasawa: Chem. Phys. Lett. Vol. 226 (1994), p. 111.

[16] S. Wendt, R. Schaub, J. Matthiesen, E. K. Vestergaard, E. Wahlström, M. D. Rasmussen, P. Thostrup, L. M. Molina, E. Lægsgaard, I. Stensgaard, B. Hammer, and F. Besenbacher: Surf. Sci. Vol. 598 (2005), p. 226.

[17] S. Morita, R. Wiesendanger, and E. Meyer (Ed.): *Noncontact Atomic Force Microscopy* (Springer, Berlin 2002).

[18] G. H. Enevoldsen, A. S. Foster, M. C. Christensen, J. V. Lauritsen, and F. Besenbacher: Phys. Rev. B Vol. 76 (2007), p. 205415.

[19] C. L. Pang, A. Sasahara, H. Onishi, Q. Chen, and G. Thornton: Phys. Rev. B Vol. 74 (2006), p. 073411.

[20] A. Fujishima, X. Zhang, and D. A. Tryk: Surf. Sci. Rep. Vol. 63 (2008), p. 515.

[21] R. Nakamura and S. Sato: J. Phys. Chem. B Vol. 106 (2002), p. 5893.

[22] G. Lu, A. Linsebigler, and J. T. Yates, Jr.: J. Chem. Phys. Vol. 102 (1995), p. 4657.

[23] G. Lu, A. Linsebigler, and J. T. Yates, Jr.: J. Chem. Phys. Vol. 102 (1995), p. 3005.

[24] C. N. Rusu and J. T. Yates, Jr.: Langmuir Vol. 13 (1997), p. 4311.

[25] W. S. Epling, C. H. F. Peden, M. A. Henderson, and U. Diebold: Surf. Sci. Vol. 412/413 (1998), p. 333.

[26] M. A. Henderson, W. S. Epling, C. L. Perkins, and C. H. F. Peden: J. Phys. Chem. B Vol. 103 (1999), p. 5328.

[27] C. L. Perkins and M. A. Henderson: J. Phys. Chem. B Vol. 105 (2001), p. 3856.

[28] M. A. Henderson: Langmuir Vol. 12 (1996), p. 5093.

[29] B. C. Gates and J. Knözinger (Ed.): Impact of Surface Science on Catalysis (Academic Press, San Diego 2000).

[30] A. Linsebigler, G. Lu, and J. T. Yates, Jr.: J. Phys. Chem. Vol. 100 (1996), p. 6631.

[31] A. Linsebigler, G. Lu, and J. T. Yates, Jr.: J. Phys. Chem. Vol. 103 (1995), p. 9438.

[32] A. Linsebigler, C. Rusu, and J. T. Yates, Jr.: J. Am. Chem. Soc. Vol. 118 (1996), p. 5284.

[33] M. Anpo: Bull. Chem. Soc. Jpn. Vol. 77 (2004), p. 1427.

[34] M. R. Hoffmann, S. T. Martin, W. Choi, and D. W. Bahnemannt: Chem. Rev. Vol. 95 (1995), p. 69.

[35] K. Domen and T. J. Chuang: Phys. Rev. Lett. Vol. 59 (1987), p. 1484.

[36] S. J. Garrett, V. P. Holbett, P. C. Stair, and E. Weitz: J. Chem. Phys. Vol. 100 (1995), p. 4615.

[37] S. J. Garrett, V. P. Holbett, P. C. Stair, and E. Weitz: J. Chem. Phys. Vol. 100 (1995), p. 4626.

[38] G. Lu, A. Linsebigler, and J. T. Yates, Jr.: J. Phys. Chem. Vol. 99 (1995), p. 7626.

[39] J. C. S. Wong, A. Linsebigler, G. Lu, J. Fan, and J. T. Yates, Jr.: J. Phys. Chem. Vol. 99 (1995) p. 335.

[40] H. Onishi, T. Aruga, C. Egawa, and Y. Iwasawa: Surf. Sci. Vol. 193 (1988), p. 33.

[41] M. A. Henderson: J. Phys. Chem. Vol. 109 (2005), p. 12062.

[42] M. A. Henderson: J. Phys. Chem. Vol. 108 (2004), p. 18932.

[43] A. Sasahara, H. Uetsuka, T. Ishibashi, and H. Onishi: J. Phys. Chem. B Vol. 107 (2003), p. 13925.

[44] A. Sasahara, H. Uetsuka, and H. Onishi: Surf. Sci. Vol. 481 (2001), p. L437.

[45] T. Ohnoa, M. Akiyoshi, T. Umebayashi, K. Asai, T. Mitsui, and M. Matsumura: Applied

Catalysis A: General Vol. 265 (2004), p. 115.

[46] Y. Ohko, A. Fujishima, and K. Hashimoto: J. Phys. Chem. B Vol. 102 (1998), p.1724.

[47] D. Brinkley and T. Engel: Surf. Sci. Vol. 415 (1998), p. L1001.

[48] D. Brinkley and T. Engel: J. Phys. Chem. B Vol. 102 (1998), p. 7596.

[49] M. Batzill, K. Katsiev, D. J. Gaspar, and U. Diebold: Phys. Rev. B Vol. 66 (2002), p. 235401.

[50] M. A. Henderson, J. M. White, H. Uetsuka, and H. Onishi: J. Am. Chem. Soc. Vol. 125 (2003), p. 14974.

[51] H. Uetsuka, H. Onishi, M. A. Henderson, and J. M. White: J. Phys. Chem. B Vol. 108 (2004), p. 10621.

[52] J. M. White and M. A. Henderson: J. Phys. Chem. B Vol. 109 (2005), p. 12417.

[53] A. Sasahara, H. Uetsuka, T. Ishibashi, and H. Onishi: J. Phys. Chem. B Vol. 107 (2003), p. 13925.

[54] H. Uetsuka, C. L. Pang, A. Sasahara, and H. Onishi: Langmuir Vol. 21 (2005), p. 11802.

[55] K. Hiehata, A. Sasahara, and H. Onishi: Nanotechnology Vol. 18 (2007), p. 084007.

[56] M. Nonnenmacher, M. P. O'Boyle, and H. K. Wickramasinghe: Appl. Phys. Lett. Vol. 58 (1991), p. 2921.

[57] S. Kitamura and M. Iwatsuki: Appl. Phys. Lett. Vol. 72 (1998), p. 3154.

[58] S. Yanagida: C. R. Chimie Vol. 9 (2006), p. 597.

[59] M. Grätzel: J. Photochem. Photobiol. A: Chem. Vol. 164 (2004), p. 3.

[60] M. Ikeda, N. Koide, L. Han, A. Sasahara, and H. Onishi: J. Phys. Chem. C Vol. 112 (2008), p. 6961.

[61] A. Sasahara, C. L. Pang, and H. Onishi: J. Phys. Chem. B Vol. 110 (2006), p. 4751.

[62] J. N. Wilson and H. Idriss: J. Am. Chem. Soc. Vol. 124 (2002), p.11284.

[63] J. N. Wilson and H. Idriss: J. Catal. Vol. 214 (2003), p. 46.

[64] L. E. Firment: Surf. Sci. Vol. 116 (1982), p. 205.

[65] X. –Q. Gong,A. Selloni, O. Dulub, P. Jacobson, and U. Diebold: J. Am. Chem. Soc. Vol. 130 (2008), p. 370.

[66] A. Sasahara, T. C. Droubay , S. A. Chambers, H. Uetsuka, and H. Onishi: Nanotechnology Vol. 16 (2005), p. S18.

[67] R. E. Tanner, A. Sasahara, Y. Liang, E. I. Altman, and H. Onishi: J. Phys. Chem. B Vol. 106 (2002), p. 8211.

[68] W. Hebenstreit, N. Ruzycki, G. S. Herman, Y. Gao, and U. Diebold: Phys. Rev. B Vol. 62 (2000), p. R16334.

[69] T. Bak, J. Nowotn, M. Rekas, and C. C. Sorrell: Int. J. Hydrogen Energ. Vol. 27 (2002), p. 991.

[70] M. A. Fox and M. T. Dulay: Chem. Rev. Vol. 83 (1995), p. 341357.

[71] T. Fukuma, K. Kobayashi, K. Matsushige, and H. Yamada: Appl. Phys. Lett. Vol. 87 (2005), p. 034101.

[72] A. Sasahara, S. Kitamura, H. Uetsuka, and H. Onishi: J. Phys. Chem. B Vol. 108 (2004), p. 15735.

[73] T. Nomoto and H. Onishi: Phys. Chem. Chem. Phys. Vol. 9 (2007), p. 5515.